Hindawi
Journal of Spectroscopy
Volume 2022, Article ID 3328477, 11 pages
https://doi.org/10.1155/2022/3328477

Research Article

Analysis of Carbon Contents and Heavy Metals in Coal Samples Using Calibration-free LIBS Technique

Muhammad Aamir Israr,[1,2] **Qamar Abbas**,[2] **Sami Ul Haq**,[2] **and Ali Nadeem**[2]

[1]*Department of Physics and Applied Mathematics, Pakistan Institute of Engineering and Applied Sciences, P.O. Nilore, Islamabad 45650, Pakistan*
[2]*National Institute of Lasers and Optronics College, Pakistan Institute of Engineering and Applied Sciences, P.O. Nilore, Islamabad 45650, Pakistan*

Correspondence should be addressed to Ali Nadeem; drali_nadeem@yahoo.com

Received 9 February 2022; Revised 22 April 2022; Accepted 5 May 2022; Published 15 June 2022

Academic Editor: Violeta Lazic

We report a compositional analysis of four coal samples collected from different mines in Pakistan and one Chinese brand. The coal samples were pelletized in the form of a disc and irradiated with a focused laser beam of fundamental (1064 nm) and second (532 nm) harmonics of Nd:YAG laser, which produced plasma on the sample surface. The plasma emissions were recorded using a broadband (200–800 nm), high-resolution spectrometer (LIBS2500plus, Ocean Optics Inc., USA), which shows that the emission spectra from 532 nm, were more intense and dense in comparison with 1064 nm spectra. The compositional analysis of coal samples was performed using the calibration-free LIBS technique, utilizing the plasma temperature and self-absorption corrected emission line intensities. The analysis yields a number of major and trace elements in coal samples, among which the concentration of carbon varies from 642 to 718 g/kg, and sulfur contents were detected as 1.1 to 7.2 g/kg. The heavy metals chromium and lead were detected in the range of 14 to153 and 210 to 252 ppm, respectively. In addition, the gross calorific value (GCV) of all the coal samples was estimated using the concentrations of carbon, hydrogen, nitrogen, oxygen, and sulfur from 26.40 to 27.18 MJ/kg, which is an important parameter to determine the coal quality and burning efficiency.

1. Introduction

Coal is one of the oldest fossil fuels which has been extensively used for power generation since the inception of the industrial revolution owning to its worldwide availability and technologically viable extraction. Besides playing a vital role in the iron and steel industry, it is also used to extract and synthesize organic and inorganic compounds in the chemical and pharmaceutical industries. The compositional analysis of coal is vital for estimating calorific value, price, and environmental impact. Currently, there are several conventional analytical techniques for qualitative and quantitative analysis, such as X-ray fluorescence (XRF), prompt gamma neutron activation analysis (PGNAA), near-infrared spectrometry (NIRS), atomic absorption spectroscopy (AAS), etc. However, these days an optical emission spectroscopy technique known as laser-induced breakdown spectroscopy (LIBS) is being used for fast and real-time elemental analysis; having an inimitable list of advantages such as real-time, simultaneous detection of all elements, remote and standoff detection capabilities, with little or no sample preparation [1–4].

In the recent past, several research articles and reviews were published on the compositional analysis of coal using the LIBS technique, and the most comprehensive studies were carried out in China. The qualitative and quantitative analyses, including carbon content in various coals, have been performed in several studies employing the commonly used partial least square (PLS), the dominant factor-based PLS, univariate and multivariate calibration models, and calibration-free technique [5–12]. Li et al. [13] investigated the dependence of experimental parameters, such as sample

preparation, lens-to-sample distance, and ambient gas, on the elemental analysis of coal samples and detected the organic (C, H, O, N) and inorganic (Ba, Ca, Ce, Cr, Fe, K, Li, Mg, Na, S, Si, Sr, Ti, and Zn) elements. Later, Li et al. [14] reported the wavelength dependence studies for the carbon content in coal using the fundamental (1064 nm) and fourth (266 nm) harmonics of Nd:YAG laser. Vera-Londono et al. [15] reported the elemental analysis of coal under ambient conditions, and from the C_2 Swan band, the vibrational temperature was estimated as 0.62 eV. Feng et al. [12] reported the elemental concentrations of thirty-three bituminous coal samples using the partial least squares (PLS) model based on the dominant factor. Haider et al. [16] demonstrated the capability of LIBS for the multi-elements (Fe, Ti, Al, Ca, Na, Cu, Zr, Nd, Yb, Ce, Ga, etc.) analysis of coal samples. Wallis et al. [17] reported the analysis of Ca, Al, Na, Fe, Mg, and Si elements by plotting the calibration curves in low ash lignite coal. Chadwick et al. [18] reported developing and commercializing a laser-induced breakdown spectroscopy system for low-ash lignite coal chemical analysis for power generation companies. Iqbal et al. [19] delineated the comparison of the Thar coal with the standard reference sample (SARM 20) using the CF-LIBS and laser ablation time of flight mass spectrometer (LA-TOF-MS) technique. Whereas, in the following article, Iqbal et al. [20] reported the percentage composition of total carbon contents along with major elements (Ca, Si, Fe, Ti, Mg, Na, K, Li, Al and C) of Lakhra coal using the CF-LIBS with self-absorption correction (IRSAC) and density correction.

In coal, the major elements C, H, O, N and S are used to determine the coal quality and burning efficiency by determining the gross calorific values (GCV). The sulfur is present in almost every kind of coal in the form of sulfate, sulfide, pyrite, organic molecular, and as an element. All these forms enter the atmosphere during combustion, causing health hazards. The sulfur detection in coal with LIBS is relatively complex due to fewer emission lines in the visible region, low emission intensity, high excitation potential, and reactivity of excited sulfur with oxygen [21]. Despite these difficulties, the scientific community has reported sufficient work on detecting and quantifying sulfur in coal, using single-pulse LIBS and double-pulse LIBS [22, 23]. At the same time, Liu et al. [24] reported the distribution, concentration, and health hazards of sulfur using chemical methods around coal mines. In addition, heavy and toxic metals are also reported in different brands of coals, such as As, Cd, Cr, Co, Hg, Pb, Ni, and Sn. These metals are transferred to fly ash and mixed with air causing soil contamination and hazards to public health. Although toxic and heavy elements exist as traces, these metals drastically affect public health, nearby soil, and plants due to large coal consumption. These metals affect the plants and may imbalance the ecosystem of coal mining areas [25]. Verma et al. [26] reported the heavy metals as Pb (0.170–0.581 ppm), Ni (0.024–0.087 ppm), Fe (0.186–11.98 ppm), Cr (0.036–0.061 ppm), and Mn (0.013–0.178 ppm) in groundwater due to the fly ash of coal-fired thermal power plant with the Energy Dispersive X-ray (EDX). According to the World Health Organization (WHO), these values exceed the guideline values. Subsequently, Yin et al. [27] reported the rapid analysis of heavy metals in the coal ash, emphasizing lead quantification using laser-induced breakdown spectroscopy.

The aim of the present research work is the comprehensive properties analysis of different coal samples used in the power plants in Pakistan. The qualitative analysis confirms the presence of major (C, N, H, O S, Ca, Al, and Si) and trace (Ba, Ce, Cr, Fe, K, Li, Mg, Mn, Na, Pb, Sr, Ti, and Zn). It is worth mentioning that S is detected in every coal sample ranging from 1.1 to 7.2 g/kg. After self-absorption corrections in emission line intensities, the calibration-free LIBS technique and its variant were applied for the quantitative analysis. The calorific value is determined for all the coal samples, which varies from 26.40 to 27.18 MJ/kg. In addition, concentrations of some heavy toxic elements Cr and Pb were also determined; therefore, these studies are critical to protecting human health from toxicity and living in the surrounding area of coal-fired plants.

2. Materials and Methods

The experimental setup was almost the same as described in previous papers [28, 29]. Briefly, the coal samples were irradiated with the laser fluence of 140 J/cm2 using the fundamental and second harmonics of a Q-switched Nd:YAG laser (Quantal Brilliant B, Twin) system. A 10 cm focal length the biconvex lens was used to focus the laser beam at approximately 1.6 mm inside the sample surface. At this position, the spot size (diameter) was 300 μm for both the 1064 nm and 532 nm laser ablation wavelengths. The spot size at 1.6 mm was obtained on a laser burn paper at low laser energy and measured using an optical microscope. The spot size at the focus was obtained using $f\lambda/\pi\omega_s$, as 7.4 μm and 3.6 μm, for 1064 and 532 nm respectively. Here, f is the focal length of the lens, λ is the ablation wavelength, and ω_s is the radius of the spot at the focusing lens. The Laser energy was measured using the (FieldMaxII-TOP, Coherent Inc., USA) power/energy meter. The coal sample was mounted on a rotation stage to change the sample position after each laser shot to enhance signal reproducibility. The emissions from plasma were recorded using the LIBS2500plus spectrometer (Ocean Optics Inc., USA) via an optical fiber of 600 μm core diameter coupled with a collimating lens for 0°–45° field of view and placed at 3 mm away from the target sample. The spectrometer was equipped with seven-channel Ocean Optics Inc., HR2000+ high-resolution modules of cumulative range from 200–800 nm with a 5 μm slit width and an optical resolution of 0.1 nm. The spectrometer was radiometrically calibrated using a DH-2000 CAL lamp, and wavelength calibration was performed using a low-pressure Mercury argon lamp. The operation of the spectrometer was controlled by OOLIBS software. The gate width of the LIBS spectrometer was fixed at 2.1 ms, which is much broader than the lifetime of the plasma; with this considerable integration time, the determination of plasma parameters is meaningless. In order to resolve this issue, Grifoni et al. [30] proposed a technique to acquire a time-resolved emission spectrum using the time-integrated spectrometer. Later, this technique was also adopted by Ahmed et al. [31] and Sun

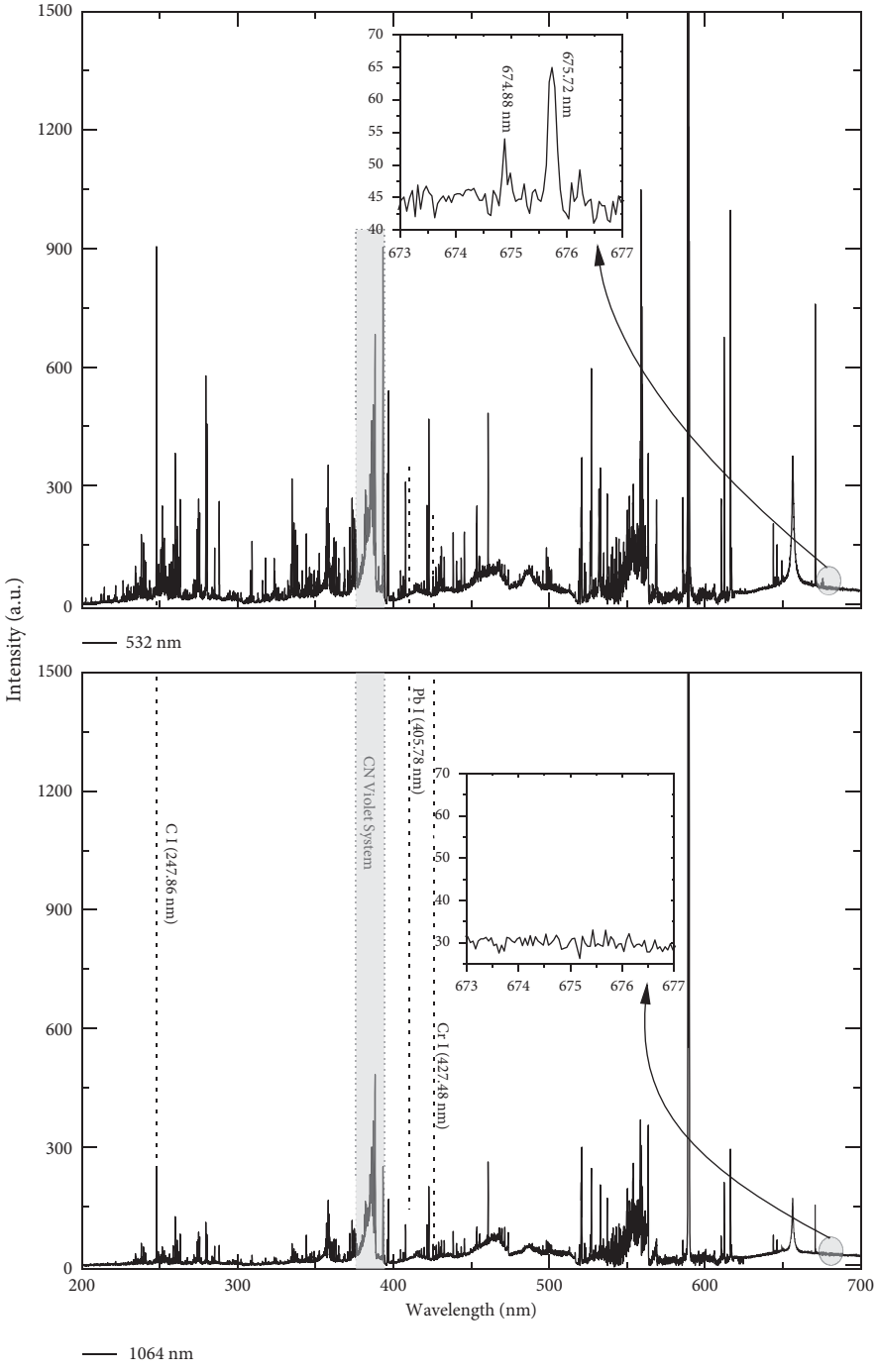

Figure 1: Comparison of emission spectra of Makerwal coal produced by irradiating laser beam of (a) 532 nm and (b) 1064 nm of Nd: YAG laser.

et al. [32]. In the present work, using this technique, two sets of data at 3.5 μs and 4.5 μs gate delay were acquired, averaged, and their difference was time-resolved spectra with an integration time of 1 μs. At this optimized integration time, plasma temperature was determined and utilized in the McWhirter criteria for the validation of local thermodynamic equilibrium (LTE). Moreover, the emission spectra were recorded with the optimized experimental parameters such as laser irradiance, the lens to sample distance, spot size on the sample surface, and detector gate delay to get the optimum signal-to-noise ratio. All the spectra were averaged of 15 laser shots to enhance the signal-to-noise ratio under similar experimental conditions.

The five coal samples collected from coal mines were cleaned with acetone and heated up to 100°C for two hours to remove moisture contents. Thereafter, the coal powdered was firstly placed in an aluminum pellet die with a diameter of 25 mm and height of 10 mm and then pressed into coal

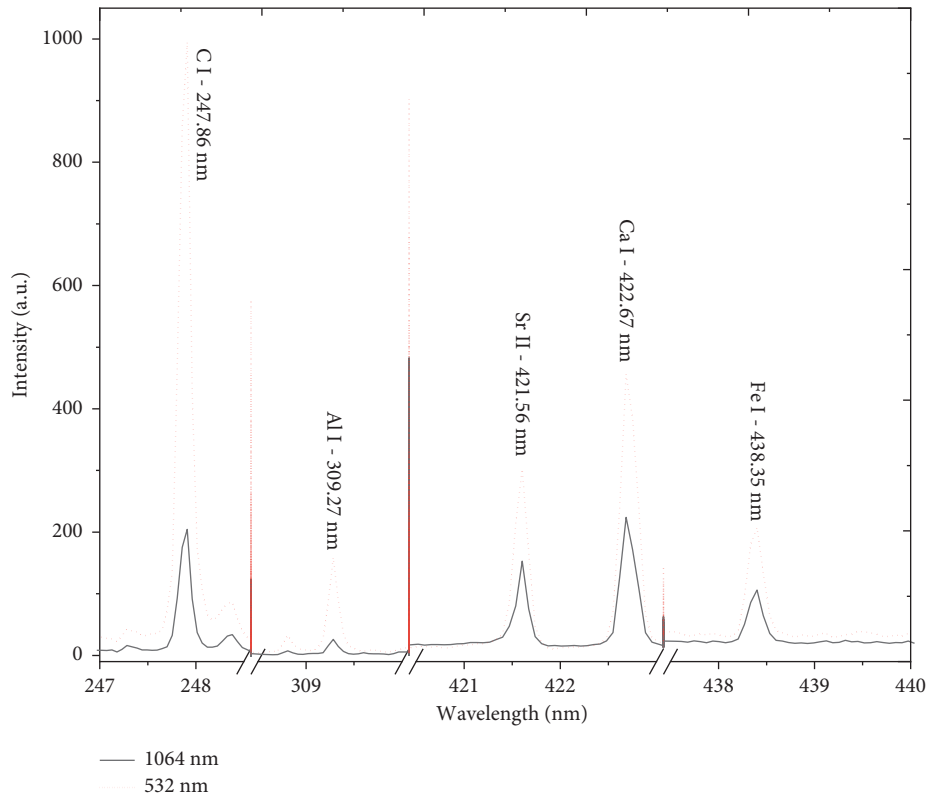

Figure 2: Enhancement in emission intensities using the 532 nm wavelength compared to the 1064 nm wavelength.

pellets at a pressure of 10-tons for 5 minutes for subsequent measurements.

3. Results and Discussion

3.1. Qualitative Analyses of Coal Samples. The qualitative analyses of five coal samples collected from different mines in Pakistan, namely Lakhra, Duki, Makerwal, Thar, and one Chinese sample collected from (District Jining, Shandong, China) were performed by recording the corresponding emission spectra from laser-induced plasma. Figure 1 shows the representative emission spectra of Makerwal coal, produced by irradiating fundamental and second harmonics of Nd:YAG laser at 100 mJ pulse energy (140 J/cm2). The comparison of the emission spectra reveals that the emission spectra of 532 nm are much more populated, and the spectral line intensities are much more intense than the 1064 nm spectra recorded at the same laser fluence. The enhanced emission intensities may be due to higher ablation and less thermal effects at shorter wavelengths [14], due to the better laser-matter coupling and less plasma shielding, as most of the pulse energy is utilized in direct bond-breaking instead of heating the target material. Furthermore, the signal enhancement due to the 532 nm is due to a relatively high photon energy of 532 nm wavelength as compared to 1064 nm to produce plasma. Also, 532 nm wavelength triggers multiphoton ionization at the start of breakdown followed by fast initiation and formation of plasma. Whereas, in the case of 1064 nm wavelength, the interaction with the target material produces strong heating and ionization of vapor which leads to plasma formation. This attributes to inverse Bremsstrahlung absorption in which free electrons gain kinetic energy for the laser beams and promote plume ionization and excitation through collisions with the excited and ground state neutrals and the plasma acts as a shield for laser radiation and the last part of the laser does not reach the target surface [14, 33–36]. This is due to the fact that the enhanced and dense emission spectra due to 532 nm ablation consist of almost all the elements present in a sample, leading to stoichiometric ablation. The emission spectra were analyzed using MATLAB® code and NIST atomic database [37] and compared with the spectra of pure elements.

In comparison to the 1064 nm spectra, the 532 nm spectra show almost five times signal enhancement in carbon emission line (247.86 nm), three times in iron (406.36 nm), two times in calcium (422.67 nm), and two times signal enhancement in strontium (421.56 nm). At 406 nm, the triplet emission lines of lead were detected with a good signal-to-noise ratio of 532 nm, whereas these lines are almost absent in the spectra of 1064 nm wavelength, as shown in Figure 2. A similar case is with the chromium line at 426.13 nm, which is on background level in the spectra of 1064 nm but detected with a good signal to noise ratio in 532 nm spectra. In coal, sulfur is usually present in trace amounts and is assumed to be in each type of coal. However, in the present work, it was not detected in the spectra of 1064 nm, but in 532 nm spectra, it was detected with a good signal-to-noise ratio at 674.88 and 675.72 nm (see Figure 1). In the higher spectral range from 650–800 nm, the H-Alpha

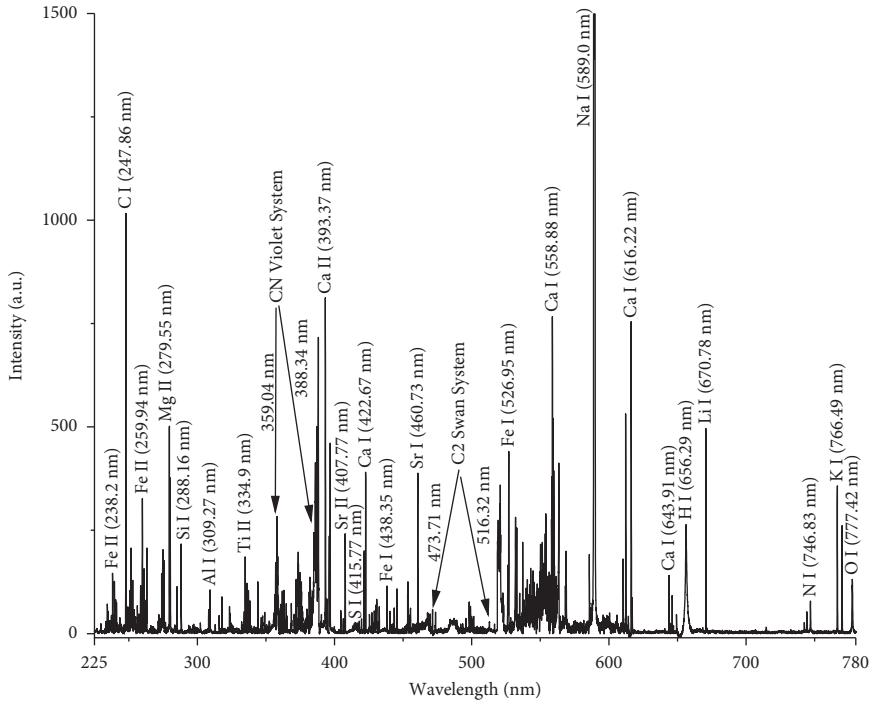

Figure 3: Portions of the emission spectrum from 225 to 780 nm with major lines and CN and C_2 molecular bands are assigned.

line at 656.29 nm, nitrogen triplet at 742.36, 744.23, and 746.83 nm, and oxygen at 777.42 nm were also identified in both spectra, but their intensities are many times higher in 532 nm laser-ablated spectra. Therefore, we have selected the emission spectra of 532 nm for the qualitative and quantitative analysis in this work. The high-intensity emission lines of neutral and singly ionized lines were assigned (see Figure 3). Most of the high-intensity lines were identified as carbon (C), hydrogen (H), nitrogen (N), aluminum (Al), calcium (Ca), oxygen (O), and silicon (Si). At the same time, minor and trace elements barium (Ba), chromium (Cr), iron (Fe), magnesium (Mg), manganese (Mn), lead (Pb), strontium (Sr), titanium (Ti), and zinc (Zn) were detected. The spectrum in Figure 3 shows that the spectrum's ultraviolet (UV) and visible regions are denser due to the presence of most elements than the higher spectral regions. The spectral part from 200 to 400 nm primarily consists of neutral lines of iron, magnesium, silicon aluminum, titanium, and a strong CN violet system was also identified at 359.04 and 388.3 nm, whereas three C_2 bands were detected on the higher energy side at 516.32, 473.71 and 468.48 nm. In the spectral range from 650–800 nm, the Hα line at 656.29 nm, nitrogen triplet at 742.36, 744.23, 746.83 nm, and oxygen at 777.42 nm were identified with good signal to noise ratio.

3.2. Quantitative Analysis Using Calibration-free LIBS. The quantitative analyses of coal samples were performed using the calibration-free LIBS technique proposed by Ciucci et al. [38], which utilizes the emission line intensities and plasma parameters instead of standard reference samples and calibration curves. Briefly, the integrated line intensities and plasma temperature are used to extract all the sample species' elemental concentrations simultaneously. As the integrated line intensity is proportional to elemental concentration through the following expression [38];

$$I_{\lambda}^{ki} = FC_s \frac{A_{ki} g_k}{U_s(T_e)} e^{-E_k/k_B T_e}. \quad (1)$$

Here I_{λ}^{ki} is the line integrated intensity of a transition having a wavelength λ and transition probability Aki. U_s (T_e) is the partition function of the emitting species at plasma temperature Te, Cs is the concentration of the emitting species s, and F is the optical efficiency of the experimental setup. This expression holds under the assumptions that (i) plasma is in local thermodynamic equilibrium (LTE), (ii) optically thin (iii), and stoichiometrically ablated, where the plasma composition is assumed to represent the actual material composition prior to ablation. The plasma temperature was determined using the Boltzmann plot method by taking the logarithm of equation (1) as follows;

$$\ln\left(\frac{I_{\lambda}^{ki}}{A_{ki} g_k}\right) = \frac{-E_k}{k_B T_e} + \ln\left(\frac{FC_s}{U_s(T_e)}\right). \quad (2)$$

The plot of $\ln(I_{\lambda}^{ki}/A_{ki} g_k)$ versus E_k is known as the Boltzmann plot, which yields the slope and intercepts when fitted with a straight-line equation. The slope gives the plasma temperature, whereas intercept is used in evaluating the species concentration. Figure 4(a) shows the Boltzmann plots, built using Fe I and II emission lines, detected in the Makerwal coal sample. The linear fitting over these data points yields the plasma temperature as 9100 ± 700 K and 8600 ± 600 K with an adjusted R^2-value of 98% and 99%. The data points in both plots are scattered around the fitted lines,

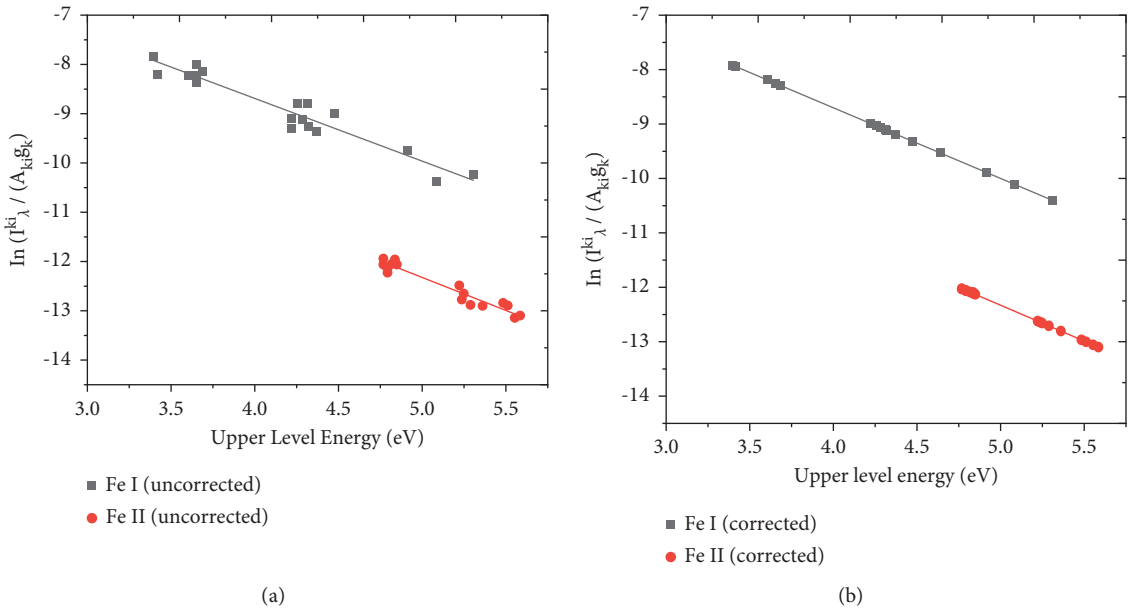

Figure 4: (a) Boltzmann plots built without self-absorption corrections of Fe I and II emission lines; the red lines linearly fit the experimental data points. (b) Boltzmann plots built with self-absorption correction on the Fe I and II emission lines; the red lines linearly fit the experimental data points.

resulting in less accurate plasma temperature and, consequently, the quantitative analysis. This may be due to the self-absorption in the emission lines, which reduces the line intensities from their actual values. Therefore, self-absorption correction in the emission lines of Fe I and II were carried out using the internal reference self-absorption correction (IRSAC) procedure [32]. In this method, the emission line with higher excitation energy of upper level and lower transition probability is considered the least self-absorbed and an internal reference line. To correct the integrated line intensities of the rest of the emission lines of an element, their intensities are compared with this reference line, which yields a new corrected set of integrated line intensities. In the present work, the Fe I and II emission lines, which were used for the determination of plasma temperature, have been corrected by using 349.78 and 266.50 nm lines, respectively, as internal reference lines, and the corrected intensities have been extracted using the following expression [32, 39, 40];

$$\overline{I_{\lambda}^{ki}} = I_{\lambda_R}^{mn} \frac{A_{ki} g_k}{A_{mn} g_m} e^{(E_m - E_k)/k_B T_e}. \quad (3)$$

Where, $I_{\lambda_R}^{mn}$ is the intensity of the reference line and A_{mn} and g_m are its transition probability and the statistical weight of the upper energy state and $\overline{I_{\lambda}^{ki}}$ is the corrected line intensity and A_{ki} and g_k are its respective parameters. Using this procedure, the self-absorption corrected emission intensities have been used to build Boltzmann plots of Fe I and II, as shown in Figure 4(b). The data points are stretched along the fitted lines, reflecting quantity fitting as a 99.9% adjusted R_2 value. In comparison with the Boltzmann plots without self-absorption correction, the corrected plots show less dispersion in data points with accurate and improved values of fitting parameters, which yield the improved value of plasma temperature as 8900 ± 100 K and 8800 ± 100 K for Fe I and Fe II, respectively. The Boltzmann plots of other elements also yield similar temperatures within uncertainty, which predict the plasma is optically thin and is in local thermodynamic equilibrium.

The uncertainty in plasma temperature is 10%, which is the accumulation of uncertainties in integrated intensities of the emission lines, transition probabilities, and the fitting procedure. The uncertainty in integrated intensity is mainly due to self-absorption, which is evaluated and corrected. In addition to these uncertainties, the relative standard deviation (RSD) in emission intensities has been evaluated. The neutral (385.92 nm) and ionized (358.56 nm) emission lines of iron show 7% and 8% RSD values, respectively, which reduced to 1% after self-absorption correction. This decrease in RSD values is significant in two ways. One is that the emission lines were actually self-absorbed, although apparently not seen as self-absorbed, which shows the necessity of self-absorption correction in emission lines. The other aspect is that the data is expected to be more repeatable after self-absorption correction as their RSD is reduced to 1%.

The electron number density was determined using the Stark broadened line profiles of K, Si, Al, and Li emission lines at 766.49, 251.8, 308.9, and 670.8 nm, respectively. The line profiles were fitted with the Voigt function, which yields the FWHM as 0.24, 0.26, 0.16, and 0.14 nm, respectively. The contribution of Doppler, collision, and pressure broadenings is almost negligible. However, the contribution of instrumental broadening was determined using the low-pressure Mercury-Argon calibration lamp (HG-1, Calibration Lamp, Ocean Optics Inc., USA) to record the emission spectrum of a narrow line of Mercury and argon. The Mercury line profile was fitted with Lorentzian function, and its FWHM gives the instrumental broadening as 0.05 nm. Therefore,

after subtracting the instrumental broadening, the deconvoluted line profile of the actual Stark broadened profile was used for the measurement of electron number density, using the following relation [41, 42];

$$n_e = \frac{\Delta\lambda_{FWHM}}{2w} \times 10^{16} cm^{-3}. \quad (4)$$

Using electron impact parameter w from literature [41], the electron number density varies from $(2.41–3.01) \times 10^{17}\,\mathrm{cm}^{-3}$. The uncertainty in electron number density is estimated as 10%, which is mainly due to the uncertainty in the electron impact parameter and line profile fitting procedure. The similar electron number density from different emission lines predicts that the plasma is optically thin and is in a local thermodynamic equilibrium state (LTE). These electron number densities and plasma temperatures were used to verify the validity of local thermodynamic equilibrium (LTE) using the Mc-Whirter criterion, using in equation (6) [41]. It is a necessary criterion but not the sufficient condition for plasma to be in local thermodynamic equilibrium and thus qualify for the compositional analysis using the CF-LIBS technique;

$$n_{e\,(\mathrm{measured})} > n_{e\,(\mathrm{calculated})}, \quad (5)$$

where

$$n_{e\,(\mathrm{calulated})} = 1.6 \times 10^{12} \sqrt{T_e} \left(\Delta E_{ki}\right)^3. \quad (6)$$

The magnesium emission line at 202.58 nm having $\Delta E_{ki} = 6.12eV$, and $T_e = 8000$ K, were used in equation (6), which yields the electron number density as $2.65 \times 10^{16}\mathrm{cm}^{-3}$. Since the measured electron density is one order of magnitude higher than the calculated value, the assumption of LTE is fulfilled in the present work, i.e., the plasma has more collisions than the radiative transitions. The plasma temperature and electron number densities of all the five coal samples have been tabulated in Table 1.

After completing all the pre-requisites of CF-LIBS, the quantitative analysis was performed using equations. (8) and (9). As the sum of the concentration of all the elements is unity, that has been used to extract the experimental parameter F, and finally, the concentration of neutral and singly ionized species has been determined using the following relations [38];

$$\sum_s C_s = \frac{1}{F} \sum_s U_s(T_e) e^{q_s} = 1, \quad (7)$$

$$C_s = \frac{U_s(T_e) e^{q_s}}{F}, \quad (8)$$

$$C_s = \frac{U_s^I(T_e) e^{q_{sI}} + U_s^{II}(T_e) e^{q_{sII}}}{F}. \quad (9)$$

Here, $U_s^I(T_e)$ and $U_s^{II}(T_e)$ are the partition functions of neutral and singly ionized species, q_{sI} and q_{sII} are the intercepts of the Boltzmann plots (see Figure 5). The Boltzmann plots in Figure 5 are drawn using self-absorption corrected emission lines of the elements (Al I, Ca I, Ca II, Fe I, Fe II, Si I, Ti I, and Ti II) which yield the intercepts at fixed plasma temperature. However, it is difficult to have sufficient emission lines of each sample species to build Boltzmann plots and extract intercepts. This issue has been resolved by Fu et al. [40] by introducing the variant of CF-LIBS, which utilizes line intensity relation to extract intercept (without Boltzmann plot) using the known value of plasma temperature. Therefore, the intercepts of the rest of the species were extracted directly from line intensity expression

Table 1: Plasma temperature and electron number densities of the coal samples.

Coal samples	Temperature (K)	Electron number density (cm^{-3}) ($\times 10^{17}$)
Chinese	8300 ± 400	2.84 ± 0.8
Lakhra	8500 ± 600	3.01 ± 0.7
Duki	8200 ± 500	2.33 ± 0.9
Makerwal	8800 ± 600	2.41 ± 0.7
Thar	7900 ± 500	2.17 ± 0.6

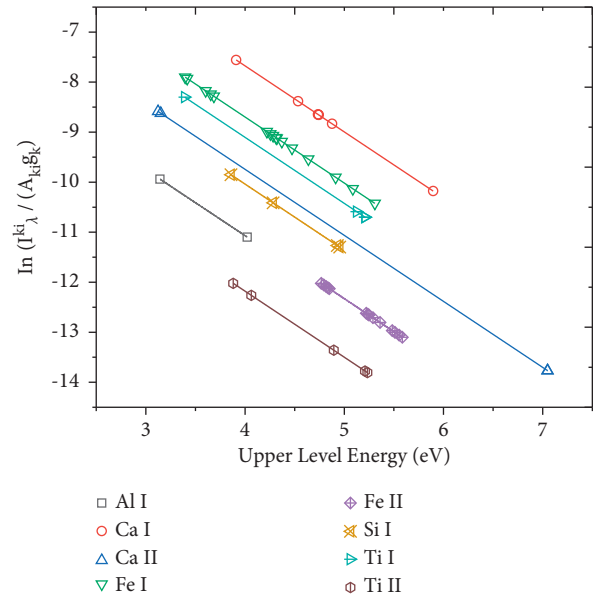

Figure 5: Combined Boltzmann plot with the self-absorption corrected emission lines of Al, Ca, Fe, Si, and Ti elements, the data points are linearly fitted to extract intercept at the fixed slope.

Table 2: Quantitative analysis of major elements in coal samples collected from coal mining sites across Pakistan and one Chinese sample.

The concentration of major elements in coal samples (g/kg)					
Elements	Chinese	Lakhra	Duki	Makerwal	Thar
Al	5.3 ± 0.2	14 ± 1.1	4.3 ± 0.2	9.1 ± 0.4	15 ± 0.7
C	**718 ± 23**	**665 ± 17**	**701 ± 22**	**642 ± 21**	**644 ± 27**
Ca	42 ± 1.4	44 ± 2.1	13 ± 0.3	41 ± 1.3	37 ± 1.2
H	34 ± 1.2	49 ± 2.1	42 ± 1.2	35 ± 1.1	52 ± 1.4
N	7.2 ± 0.2	20 ± 1	12 ± 0.2	11 ± 0.3	13 ± 1.1
O	188 ± 6	193 ± 6	225 ± 9	194 ± 6	222 ± 7
S	**2.1 ± 0.2**	**7.3 ± 0.3**	**1.1 ± 0.1**	**52 ± 2.1**	**5.2 ± 0.2**
Si	1.2 ± 0.1	2.1 ± 0.2	1.3 ± 0.1	5.4 ± 0.2	7.1 ± 0.4

Table 3: Quantitative analysis of minor elements in coal samples collected from coal mining sites across Pakistan and one Chinese coal sample.

The concentration of minor elements in coal samples (ppm)					
Elements	Chinese	Lakhra	Duki	Makerwal	Thar
Ba	63 ± 6	37 ± 6	—	54 ± 8	53 ± 7
Ce	—	—	—	—	20 ± 7
Cr	—	**70 ± 8**	—	**153 ± 12**	**14 ± 6**
Fe	—	674 ± 21	—	3190 ± 123	1147 ± 37
K	316 ± 11	594 ± 20	833 ± 24	649 ± 20	749 ± 24
Li	574 ± 18	338 ± 17	291 ± 11	620 ± 33	458 ± 27
Mg	701 ± 27	207 ± 24	255 ± 31	3680 ± 106	379 ± 43
Mn	147 ± 21	137 ± 14	137 ± 17	—	166 ± 16
Na	1861 ± 58	736 ± 18	93 ± 11	1020 ± 32	978 ± 30
Pb	—	—	**252 ± 27**	**210 ± 29**	—
Sr	—	777 ± 31	—	405 ± 13	566 ± 16
Ti	—	1391 ± 41	—	1154 ± 43	906 ± 29
Zn	33 ± 8	—	—	—	70 ± 13

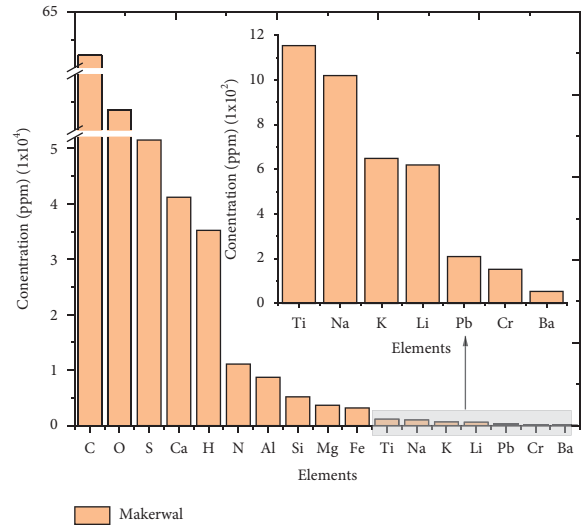

Figure 6: Elemental concentration of Makerwal coal showing both major and minor elements, the inset shows the concentration of trace metals detected in coal.

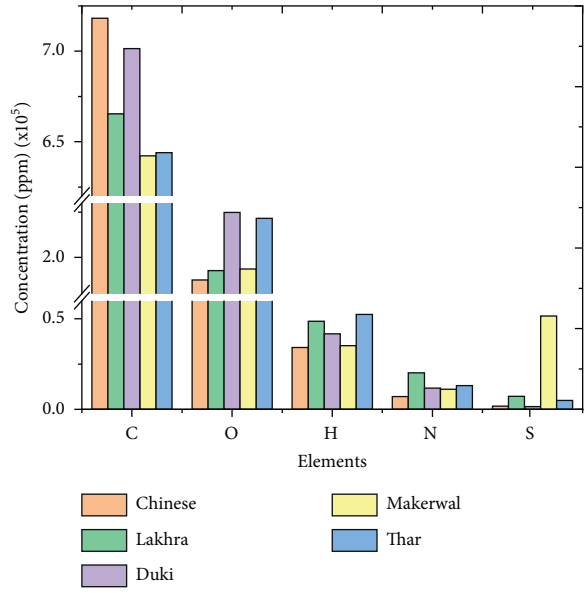

Figure 7: Concentration of major elements C H, N S, and O in the five coal samples.

(equation (1) provided that plasma temperature is known. This variant of the CF-LIBS approach was employed by various groups, including our group, for the quantitative analysis of trace elements in alloy and solar cells [29, 43].

Adopting this procedure, the concentration of carbon, heavy metals, and other constituents in Makerwal coal have been determined, which are enlisted in Tables 2 and 3 and illustrated as bar graphs in Figure 6. The elements in this figure are in descending order, showing that carbon is the most abundant element with 642 ± 21 g/kg, followed by oxygen, sulfur, calcium, etc. The carbon is the major element, whereas sulfur is detected in the Makerwal coal sample with a concentration of 52 ± 2.1 g/kg. The low concentration elements are shown as inset, among which chromium and lead are quantified as 153 ± 12 ppm and 210 ± 29 ppm, respectively. The quantitative analysis was extended to four more coal samples, namely Thar, Duki, Lakhra, and one Chinese. The results of all these samples are also listed in Tables 2 and 3 and illustrated in Figure 7. This figure contains the concentration of important coal constituents detected in all five coal samples. The carbon concentration varies from 642 to 718 g/kg, with the maximum concentration found in Chinese coal, whereas Makerwal coal has the relatively least concentration (642 g/kg). In an earlier investigation, Iqbal et al. [19] reported higher carbon contents of 84% (840 g/kg) in Thar coal. In the subsequent paper, Iqbal et al. [20] reported the corban contents in Lakhra coal using three different approaches as 96.3 ± 5.1, 87.8 ± 3.5, and 89.3 ± 3.5%, which is almost comparable to the Thar coal.

In comparison, Anjum et al. [44] reported the concentration of carbon contents as 55.7% (557 g/kg), which is almost comparable to the Lakhra coal as evaluated in the present work at 665 g/kg. This difference in concentration may be due to sample collection from different locations and depths of coal mines. The contents of oxygen, hydrogen, and nitrogen are present almost with the same concentration in all the five coals; however, sulfur ranges from 1.1 to 7.3 g/kg, with a maximum value in Lakhra coal. Unfortunately, due to the unavailability of the ICP-MS system, it was not possible to validate our results with the conventional standard technique. Whereas in our previous work on the quantitative analysis of standard Al alloy sample was performed using the CF-LIBS technique, the results were validated with the certified values of the reference standard material (SRM) which are in good agreement as reported by Shakeel et al. [29]. Recently, one of the co-author, Qasim et al. [45], applied CF-LIBS and ICP-MS techniques to quantitatively analyze the mineral profile in the Maerua oblongifolia plant, and the results are in close agreement.

It is well known that coal is the cheapest energy source; however, it causes air pollution in the form of smoke exiting from stacks which contaminate air and soil due to the

presence of toxic elements As, Cd, Cr, Co, Hg, Pb, Ni, and Sn, in coal fumes. Although these metals exist in trace amounts but due to large coal consumption, these metals drastically affect public health [27, 46]. For example, lead and chromium in coal produce a large amount of toxins in the environment, which may cause carcinoma, infertility, cardiovascular diseases, respiratory problems, skin and eye diseases [8, 9]. The present work evaluated the concentration of toxic metals in all five coal samples with the calibration-free LIBS technique, and the results are summarized in Tables 2 and 3. The analysis shows that in Lakhra, Makerwal, and Thar coals, Cr is detected from 70, 153, and 14 ppm, respectively, whereas Pb is present in Duki (252 ppm), and Makerwal (210 ppm) coal samples. The sulfur is detected in all coal samples; however, its concentration varies from 7.3 ± 0.3 to 1.1 ± 0.1 g/kg. Although sulfur contributes to the burning efficiency of coal due to its oxidation, at the same time, it is toxic, i.e., the sulfur oxides are greenhouse gases that cause toxic acid rain, pose numerous health hazards, and enhance the corrosion process [40]. It is due to these harmful effects; that the coal mining sites having less concentration of toxic elements are economically beneficial [44].

Finally, the gross calorific value (GCV) of all the coal samples was estimated, which is an essential parameter for determining coal quality and its burning efficiency; it is the total heat released from the complete combustion of coal [47]. The GCV of all the five coal samples was determined utilizing the percentage concentration of carbon, hydrogen, nitrogen, oxygen, and sulfur in the following expression [47];

$$GCV = 0.35\,(C) + 1.16\,(H) + 0.06\,(N) + 0.06\,(S) - 0.11\,(O)\text{MJ/kg}. \quad (10)$$

The gross calorific values of coal samples range from 26.40 to 27.18 MJ/kg. The average gross calorific value is 26.96 MJ/kg, which is comparable to most of the earlier reported values. Chinese coal has the highest gross calorific value (27.18 MJ/kg), whereas Thar coal with 26.40 MJ/kg has the minimum value. Previously, Yuan et al. [7] reported the earlier calorific values in the range 17.74–29.07 MJ/kg, whereas Li et al. [48] reported18.70 to 32.58 MJ/kg using the LIBS technique and the PLS model. Later, Zhang et al. [49] determined the ash content, volatile matter, and calorific value of coal ash samples. Their reported calorific values are in the range of 16.86–28.51 MJ/kg.

4. Conclusion

Compositional analysis of five coal samples collected from various coal mines across Pakistan and one Chinese coal has been carried out using calibration-free LIBS and its variant using self-absorption corrected line intensities. The compositional analysis confirms the presence of some major elements (C, H, N, S, O, Al, Ca, and Si) as well as minor (Ba, Ce, Cr, Fe, K, Li, Mg, Mn, Na, Pb, Sr, Ti, and Zn) elements. The carbon is the most abundant element having a concentration from 642–718 g/kg, whereas the concentration of sulfur varies from 1.1 to 7.2 g/kg. Concentrations of C, H, N, S, and O were used to determine the gross calorific value of all the samples, which varies from 26.40 to 27.18 MJ/kg. These studies are critical to extending our experimental capabilities toward developing a compact system for online coal quality monitoring in mines and power plants.

Data Availability

The data used to support the findings of this study are available from the corresponding author upon reasonable request.

Conflicts of Interest

The authors declare that they have no conflicts of interest.

Acknowledgments

Mr. Muhammad Aamir Israr is grateful to the Higher Education Commission (HEC), Pakistan, for the award of M.Phil. Leading to Ph.D. studies financial support under the HEC Indigenous 5000 Fellowship Program Phase-II (Grant No. 112-26342-2PS1-039).

References

[1] I. E. Agency, *Coal Information 2018*, International Energy Agency, Paris, France, 2018.

[2] D. A. Cremers and L. J. Radziemski, *Handbook of Laser-Induced Breakdown Spectroscopy*, John Wiley & Sons, West Sussex, UK, 2nd edition, 2013.

[3] R. Noll, *Laser-Induced Breakdown Spectroscopy*, Springer, Berlin, Germany, 2012.

[4] D. W. Hahn and N. Omenetto, "Laser-induced breakdown spectroscopy (LIBS), Part I: review of basic diagnostics and plasma—particle interactions: still-challenging issues within the analytical plasma community," *Applied Spectroscopy*, vol. 64, no. 12, pp. 335A-336A, 2010.

[5] D. W. Hahn and N. Omenetto, "Laser-induced breakdown spectroscopy (LIBS), Part II: review of instrumental and methodological approaches to material analysis and applications to different fields," *Applied Spectroscopy*, vol. 66, no. 4, pp. 347–419, 2012.

[6] J. El Haddad, L. Canioni, and B. Bousquet, "Good practices in LIBS analysis: review and advices," *Spectrochimica Acta Part B: Atomic Spectroscopy*, vol. 101, pp. 171–182, 2014.

[7] T. Yuan, Z. Wang, S.-L. Lui et al., "Coal property analysis using laser-induced breakdown spectroscopy," *Journal of Analytical Atomic Spectrometry*, vol. 28, no. 7, pp. 1045–1053, 2013.

[8] X.-L. C. Feng-Zhong Dong, X. L. Chen, Q. Wang et al., "Recent progress on the application of LIBS for metallurgical online analysis in China," *Frontiers of Physics*, vol. 7, no. 6, pp. 679–689, 2012.

[9] S. Sheta, M. S. Afgan, Z. Hou et al., "Coal analysis by laser-induced breakdown spectroscopy: a tutorial review," *Journal*

of Analytical Atomic Spectrometry, vol. 34, no. 6, pp. 1047–1082, 2019.

[10] S. Legnaioli, B. Campanella, S. Pagnotta, F. Poggialini, and V. Palleschi, "Determination of ash content of coal by laser-induced breakdown spectroscopy," *Spectrochimica Acta Part B: Atomic Spectroscopy*, vol. 155, pp. 123–126, 2019.

[11] Y. Zhang, M. Dong, L. Cheng, L. Wei, J. Cai, and J. Lu, "Improved measurement in quantitative analysis of coal properties using laser induced breakdown spectroscopy," *Journal of Analytical Atomic Spectrometry*, vol. 35, no. 4, pp. 810–818, 2020.

[12] J. Feng, Z. Wang, L. West, Z. Li, and W. Ni, "A pls model based on dominant factor for coal analysis using laser-induced breakdown spectroscopy," *Analytical and Bioanalytical Chemistry*, vol. 400, no. 10, pp. 3261–3271, 2011.

[13] J. Li, J. Lu, Z. Lin et al., "Effects of experimental parameters on elemental analysis of coal by laser-induced breakdown spectroscopy," *Optics & Laser Technology*, vol. 41, no. 8, pp. 907–913, 2009.

[14] X. Li, Z. Wang, Y. Fu, and W. Ni, "Wavelength dependence in the analysis of carbon content in coal by nanosecond 266 nm and 1064 nm laser induced breakdown spectroscopy," *Plasma Science and Technology*, vol. 17, no. 8, pp. 621–624, 2015.

[15] L. P. Vera-Londoño, J. A. Pérez-Taborda, and H. Riascos-Landázuri, "Spectroscopic analysis of coal plasma emission produced by laser ablation," *Revista Facultad de Ingeniería Universidad de Antioquia*, vol. 78, no. 78, pp. 69–72, 2015.

[16] A. F. M. Y. Haider, M. A. Rony, R. S. Lubna, and K. Abedin, "Detection of multiple elements in coal samples from Bangladesh by laser-induced breakdown spectroscopy," *Optics & Laser Technology*, vol. 43, no. 8, pp. 1405–1410, 2011.

[17] F. J. Wallis, B. L. Chadwick, and R. J. S. Morrison, "Analysis of lignite using laser-induced breakdown spectroscopy," *Applied Spectroscopy*, vol. 54, no. 8, pp. 1231–1235, 2000.

[18] B. L. Chadwick and D. Body, "Development and commercial evaluation of laser-induced breakdown spectroscopy chemical analysis technology in the coal power generation industry," *Applied Spectroscopy*, vol. 56, no. 1, pp. 70–74, 2002.

[19] S. M. Z. Iqbal, Z. Uddin, N. Ahmed, Z. A. Umar, and M. A. Baig, "On the compositional analysis of coal using calibration free laser induced breakdown spectroscopy," *Laser Physics*, vol. 29, no. 3, Article ID 36101, 2019.

[20] S. M. Z. Iqbal, Z. Uddin, Z. A. Umar, N. Ahmed, R. Ahmed, and M. A. Baig, "Analysis of Lakhra coal by calibration free laser-induced breakdown spectroscopy (CF-LIBS) and comparison of self-absorption correction procedures," *Analytical Letters*, vol. 55, pp. 11–23, 2021.

[21] L. Dudragne, P. Adam, and J. Amouroux, "Time-resolved laser-induced breakdown spectroscopy: application for qualitative and quantitative detection of fluorine, chlorine, sulfur, and carbon in air," *Applied Spectroscopy*, vol. 52, no. 10, pp. 1321–1327, 1998.

[22] V. S. Burakov, N. V. Tarasenko, M. I. Nedelko, V. Kononov, N. Vasilev, and S. Isakov, "Analysis of lead and sulfur in environmental samples by double pulse laser induced breakdown spectroscopy," *Spectrochimica Acta Part B: Atomic Spectroscopy*, vol. 64, no. 2, pp. 141–146, 2009.

[23] Y. Ma, W. Zhang, Z. Xiong et al., "Accurate sulfur determination of coal using double-pulse laser-induced breakdown spectroscopy," *Journal of Analytical Atomic Spectrometry*, vol. 35, no. 7, pp. 1458–1463, 2020.

[24] G. Liu, Z. Peng, P. Yang, and G. Wang, "Sulfur in coal and its environmental impact from Yanzhou mining district, China," *Chinese Journal of Geochemistry*, vol. 20, no. 3, pp. 273–281, 2001.

[25] B. J. Alloway, "Heavy metals in soils: trace metals and metalloids in soils and their bioavailability," in *Environmental Pollution*, B. J. Alloway, Ed., Springer, Berlin, Germanys, 3rd edition, 2013.

[26] C. Verma, S. Madan, and A. Hussain, "Heavy metal contamination of groundwater due to fly ash disposal of coal-fired thermal power plant, Parichha, Jhansi, India," *Cogent Engineering*, vol. 3, no. 1, Article ID 1179243, 2016.

[27] W. Yin, Y. Liu, F. Zhou, R. Zhu, Q. Zhang, and F. Jin, "Rapid analysis of heavy metals in the coal ash with laser-induced breakdown spectroscopy," *Optik*, vol. 174, pp. 550–557, 2018.

[28] Q. Abbas, M. A. Israr, S. U. Haq, and A. Nadeem, "Exploiting calibration free laser-induced breakdown spectroscopy (CF-LIBS) for the analysis of food colors," *Optik*, vol. 236, Article ID 166531, 2021.

[29] H. Shakeel, S. U. Haq, V. Contreras, Q. Abbas, and A. Nadeem, "Analysis of alloy and solar cells with double-pulse calibration-free laser-induced breakdown spectroscopy," *Optik*, vol. 211, Article ID 164627, 2020.

[30] E. Grifoni, S. Legnaioli, M. Lezzerini, G. Lorenzetti, S. Pagnotta, and V. Palleschi, "Extracting time-resolved information from time-integrated laser-induced breakdown spectra," *Journal of Spectroscopy*, vol. 2014, Article ID 849310, 5 pages, 2014.

[31] R. Ahmed, N. Ahmed, J. Iqbal, and M. A. Baig, "An inexpensive technique for the time resolved laser induced plasma spectroscopy," *Physics of Plasmas*, vol. 23, no. 8, Article ID 83101, 2016.

[32] L. Sun and H. Yu, "Correction of self-absorption effect in calibration-free laser-induced breakdown spectroscopy by an internal reference method," *Talanta*, vol. 79, no. 2, pp. 388–395, 2009.

[33] E. M. Cahoon and J. R. Almirall, "Wavelength dependence on the forensic analysis of glass by nanosecond 266 nm and 1064 nm laser induced breakdown spectroscopy," *Applied Optics*, vol. 49, no. 13, pp. C49–C57, 2010.

[34] C. Barnett, E. Cahoon, and J. R. Almirall, "Wavelength dependence on the elemental analysis of glass by laser induced breakdown spectroscopy," *Spectrochimica Acta Part B: Atomic Spectroscopy*, vol. 63, no. 10, pp. 1016–1023, 2008.

[35] N. Elsherbiny and O. Aied Nassef, "Wavelength dependence of laser induced breakdown spectroscopy (LIBS) on questioned document investigation," *Science & Justice*, vol. 55, no. 4, pp. 254–263, 2015.

[36] N. M. Shaikh, M. S. Kalhoro, A. Hussain, and M. Baig, "Spectroscopic study of a lead plasma produced by the 1064nm, 532nm and 355nm of a Nd:YAG laser," *Spectrochimica Acta Part B: Atomic Spectroscopy*, vol. 88, pp. 198–202, 2013.

[37] A. Kramida, Y. Ralchenko, J. Reader, and NIST ASD Team, *Nist Atomic Spectra Database*, https://www.nist.gov/pml/atomic-spectra-database, 2019.

[38] A. Ciucci, M. Corsi, V. Palleschi, S. Rastelli, A. Salvetti, and E. Tognoni, "New procedure for quantitative elemental analysis by laser-induced plasma spectroscopy," *Applied Spectroscopy*, vol. 53, no. 8, pp. 960–964, 1999.

[39] A. Ciucci, V. Palleschi, S. Rastelli, A. Salvetti, D. Singh, and E. Tognoni, "Cf-lips: a new approach to lips spectra analysis," *Laser and Particle Beams*, vol. 17, no. 4, pp. 793–797, 1999.

[40] H. Fu, F. Dong, H. Wang, J. Jia, and Z. Ni, "Calibration-free laser-induced breakdown spectroscopy (CF-LIBS) with

standard reference line for the analysis of stainless steel," *Applied Spectroscopy*, vol. 71, no. 8, pp. 1982–1989, 2017.

[41] H. R. Griem, *Spectral Line Broadening by Plasmas*, Academic Press, New York, NY, USA, 1974.

[42] J. P. Singh and S. N. Thakur, *Laser-induced Breakdown Spectroscopy*p. 620, 2nd edition, Elsevier, Amsterdam, Netherlands, 2020.

[43] E. Tognoni, G. Cristoforetti, S. Legnaioli et al., "A numerical study of expected accuracy and precision in calibration-free laser-induced breakdown spectroscopy in the assumption of ideal analytical plasma," *Spectrochimica Acta Part B: Atomic Spectroscopy*, vol. 62, no. 12, pp. 1287–1302, 2007.

[44] G. Anjum and M. N. Khan, "The power generation from coal in Pakistan: assessment of physicochemical pollutant indicators in indigenous reserves in comparison to the foreign coal," *Pakistan Journal of Analytical & Environmental Chemistry*, vol. 18, no. 1, pp. 54–63, 2017.

[45] M. Qasim, M. Anwar-ul-Haq, A. Shah et al., "Self-absorption effect in calibration-free laser-induced breakdown spectroscopy: analysis of mineral profile in maerua oblongifolia plant," *Microchemical Journal*, vol. 175, Article ID 107106, 2022.

[46] C.-L. Chou, "Sulfur in coals: a review of geochemistry and origins," *International Journal of Coal Geology*, vol. 100, pp. 1–13, 2012.

[47] D. M. Mason and K. N. Gandhi, "Formulas for calculating the calorific value of coal and coal chars: development, tests, and uses," *Fuel Processing Technology*, vol. 7, no. 1, pp. 11–22, 1983.

[48] W. Li, J. Lu, M. Dong et al., "Quantitative analysis of calorific value of coal based on spectral preprocessing by laser-induced breakdown spectroscopy (LIBS)," *Energy and Fuels*, vol. 32, no. 1, pp. 24–32, 2018.

[49] W. Zhang, Z. Zhuo, P. Lu et al., "LIBS analysis of the ash content, volatile matter, and calorific value in coal by partial least squares regression based on ash classification," *Journal of Analytical Atomic Spectrometry*, vol. 35, no. 8, pp. 1621–1631, 2020.